Boundary-Layer Meteorology manuscript No.
(will be inserted by the editor)

Observations of near-surface heat flux and temperature profiles through the early evening transition over contrasting surfaces

Derek D. Jensen · Daniel F. Nadeau · Sebastian W. Hoch · Eric R. Pardyjak

Received: Draft October 15, 2014 / Accepted:

Abstract Near-surface turbulence data from the Mountain Terrain Atmospheric Modeling and Observations (MATERHORN) program are used to study counter-gradient heat fluxes through the early evening transition. Two sites, subjected to similar large-scale forcing but with vastly different surface and subsurface characteristics, are considered. The Playa site is located over a large desert playa with high soil moisture and no vegetation. The Sagebrush site is located over desert steppe with sparse vegetation and little soil moisture. The observed counter-gradient heat flux is found to be site and height dependent. At the Sagebrush site, the counter-gradient flux at 5 m and below occurs when the sensible heat flux reversal precedes the local temperature gradient reversal. For 10 m and above, the counter-gradient flux occurs when the sensible heat flux reversal follows the local temperature gradient reversal. At the Playa site, the counter-gradient flux at all tower heights occurs when the flux reversal follows the local gradient reversal. The phenomenon is discussed in terms of the mean temperature and heat flux evolution. The temperature gradient reversal is a top-down process while the flux reversal occurs nearly simultaneously at all heights.

D. D. Jensen
University of Utah
Department of Mechanical Engineering
Salt Lake City, UT USA 84112
E-mail: derek591@gmail.com

D. F. Nadeau
Polytechnique Montréal
Department of Civil, Geological and Mining Engineering
Montréal, QC, Canada

S. W. Hoch
University of Utah
Department of Atmospheric Sciences
Salt Lake City, UT USA 84112

E. R. Pardyjak
University of Utah
Department of Mechanical Engineering
Salt Lake City, UT USA 84112

The differing counter-gradient behaviour is primarily due to the differing subsurface characteristics between the two sites. The combined high volumetric heat capacity and high thermal conductivity of the Playa site lead to weak temperature gradients that affect the relative strength of terms in the heat flux tendency equation. A critical ratio of the gradient production to buoyant production of sensible heat flux is suggested to predict the counter-gradient behaviour.

Keywords Counter-gradient heat flux · Heat flux evolution · Similarity theory · Surface layer · Temperature evolution

1 Introduction

Under idealized, fair-weather daytime conditions, a well-mixed convective layer exists above an unstable surface layer. Within the surface layer, fluxes are considered to be constant with height and shear production of turbulence is important. Eddies generated from surface heating pass through the surface layer and impart energy into the mixed layer from below. Additionally, warm dry air is entrained from the free atmosphere, feeding energy and mass into the mixed layer throughout the day (Fedorovich et al., 2001; Pino et al., 2003; Angevine, 2007). Under nocturnal conditions, a stable boundary layer, characterized by weak and possibly intermittent turbulence and strong stratification, develops near the surface. The mixed layer becomes decoupled from the surface and decays into a residual layer, characterized by neutral stratification and weak turbulence (Stull, 1988; Mahrt et al., 1998; Mahrt, 1999). While the structure of the daytime and nocturnal boundary layers are fairly well understood, relatively little is known about the transition from daytime to nocturnal conditions. Adopting the terminology of Nadeau et al. (2011), this transition is broken into two portions. The afternoon transition begins when the surface sensible heat flux begins to decrease from its midday maximum followed by the evening transition when the surface sensible heat flux becomes negative. The early evening transition (EET) is the 1 to 2 h period before and after the heat flux reversal. Many researchers have noted that a greater understanding of the EET is important for model development and better forecasts for wind energy production, convective storm initiation, and pollutant dispersion (e.g. Cole and Fernando, 1998; Sorbjan, 1997; Acevedo and Fitzjarrald, 2003; Edwards et al., 2006; Angevine, 2007; Nadeau et al., 2011; Lothon and Lenschow, 2011; Lothon et al., 2014).

During the EET, the flow is inherently unsteady. Turbulence is non-stationary, fluxes are small and the driving forces evolve on short time scales. Furthermore, during this transition period, a well-defined surface layer and mixed layer do not exist (Grant, 1997). A variety of weak forcings drive the physics, turbulent mixing decreases and horizontal heterogeneity and differential cooling become increasingly important. Also, the traditional daytime scaling laws for the convective boundary layer (Deardorff, 1970) and surface layer (Monin and Obukhov, 1954) are no longer well-defined. Finally, after the surface sensible heat flux has reversed, entrainment fluxes continue to feed energy into the boundary layer for some time (Nieuwstadt and Brost, 1986; Sorbjan, 1997; Grimsdell and Angevine, 2002; Pino et al., 2006).

These factors combined with a relative lack of observations make a thorough analysis of the EET difficult.

Until recently, the EET was rarely studied. Starting with the work of Nieuwstadt and Brost (1986), a number of LES studies have been conducted to understand the decay of the convective boundary layer. Over the years, the studies have increased in complexity and allowed for more realistic forcing time scales and boundary conditions (Sorbjan, 1997; Acevedo and Fitzjarrald, 2001; Brown et al., 2002; Edwards et al., 2006; Kumar et al., 2006; Pino et al., 2006; Goulart et al., 2010; Kumar et al., 2010; Rizza et al., 2013; Taylor et al., 2014). Additionally, a number of laboratory experiments have been conducted to study transitional stability (Comte-Bellot and Corrsin, 1971; Cole and Fernando, 1998; Kang et al., 2003). To a lesser extent, observations are beginning to be used to study the decay of convective turbulence. Acevedo and Fitzjarrald (2001) utilized a dense sensor network to study temporal and spatial variability in mean variables through the EET, Nadeau et al. (2011) used field data to successfully model the decay of turbulent kinetic energy in a convective surface layer over contrasting surface types. Later, the Boundary Layer Late Afternoon and Sunset Turbulence (BLLAST) campaign was specifically designed to experimentally study the EET (Lothon et al., 2014). Perhaps the only field study to specifically study near-surface, counter-gradient behaviour during the EET is the BLLAST study conducted by Blay-Carreras et al. (2014). Their work found a persistent time lag between the time of the buoyancy flux reversal and local gradient reversal. Typical lag times persisted between 30 and 80 minutes. They concluded that the phenomena might be site-dependent and that further studies were necessary. In light of this and the fact that nearly all numerical weather models assume that surface fluxes are directed down-gradient (Mahrt, 1999), this topic merits further study.

Here, we build upon the work of Blay-Carreras et al. (2014) by contrasting two experimental sites that strongly differ from the one used in their study. First, the Playa site is located on a large alkaline playa with no vegetation, shallow water table and high soil moisture. Second, the Sagebrush site is located over desert steppe with limited soil moisture. We use turbulence data collected in the atmospheric surface layer to study the evolution of near-surface heat-flux and temperature-gradient profiles through the EET. The goal of this study is to provide additional clarity regarding the evolution of near-surface heat flux and temperature gradients through the EET.

2 Methods

Data for the analysis were collected during the Mountain Terrain Atmospheric Modeling and Observations Program. The principal objective of MATERHORN is to improve weather predictability in regions of complex terrain. The experimental portion of the program consisted of two field campaigns that took place at the United States Army Facility, Dugway Proving Ground in Utah's West Desert, USA. The first field campaign ran from 26 September – 7 November 2012 and focused on quiescent conditions with minimal synoptic forcing. The second campaign ran from 1 May – 6 June 2013 with an emphasis on synoptic flows. Through both campaigns, continuous observations of the near-surface wind and temperature profiles and the surface

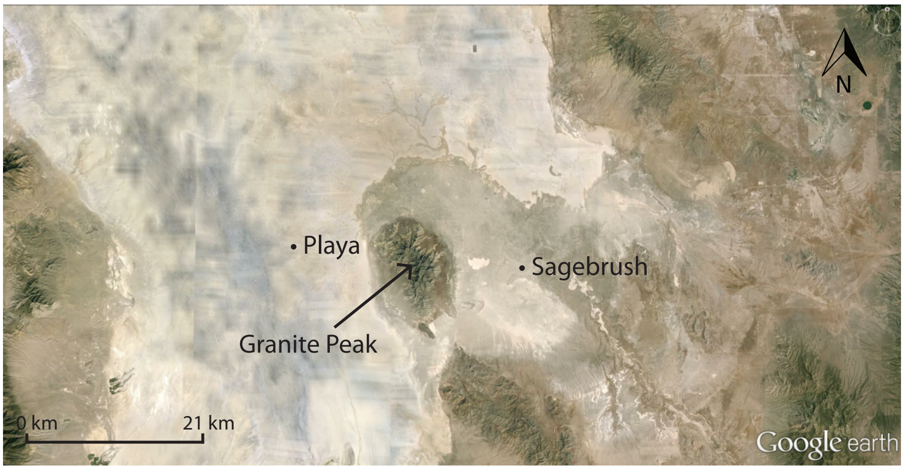

Fig. 1 Map of the two experimental sites (Google Earth, 2013).

energy balance were made. During 24 h intensive observation periods (IOPs), additional instrumentation such as tethered and free flying balloons, aircraft, lidars, hot wire anemometers, and infrared cameras were deployed. Both campaigns consisted of ten IOPs. Full details and objectives of the MATERHORN program are found in Fernando et al. (submitted to *Bull. Amer. Meteorol. Soc.*).

2.1 Experimental Sites

For the current study, we consider two highly instrumented sites, with their mean soil and surface characteristics reported in Table 1. First, the Playa site is located on a large desert playa (part of the dry remnants of the ancient Lake Bonneville) with no vegetation and an elevation of 1296 m above sea level (40°8'5.9" N, 113°27'7.8" W). The playa surface and soil characteristics are nearly homogeneous following rain events with a gradual increase in spatial heterogeneity until another rain event occurs. At depths beyond 60 mm, the playa soil is nearly always saturated. Due to high soil salinity at the Playa site, the volumetric water content (VWC) measurements were made by hand. The fall measurements were conducted only three times at a single location while the spring measurements were conducted every IOP at 20 locations (Hang et al., submitted to *Boundary-Layer Meteorol.*). Thus, a direct comparison between the fall and spring VWC is impossible. Based on the surface albedo (a), thermal conductivity (k) and volumetric heat capacity of the soil defined as $C = \rho * c$ where ρ is density and c is specific heat capacity, it is evident the mean soil moisture at the Playa was higher during the fall campaign than the spring. Under quiescent, convective conditions, an up-valley northerly flow develops. There is a typical calm period associated with sunset followed by the development of a down-valley southerly flow with a jet-like structure through much of the night.

The Sagebrush site is located approximately 25 km to the east of the Playa site (40°7'16.9" N, 113°7'44.7" W) at an elevation of 1316 m above sea level. The two sites are separated by Granite Peak, a small mountain with a maximum elevation of 850 m above the valley floor (Fig. 1). The vegetation is predominately Greasewood (Emrick and Hill, 1999) on the order of 1 m tall. The VWC is much lower at the Sagebrush site, allowing for a smaller heat capacity and thermal inertia (TI). Contrary to the Playa site, the mean soil moisture at Sagebrush is higher during the spring campaign. Additionally, the leaf area index (LAI) increases and subsequently decreases the mean surface albedo. Under quiescent, daytime conditions a north-westerly breeze develops; following the calm associated with transition, a southerly drainage flow develops with the formation of occasional low-level jets.

Table 1 Soil and surface characteristics at the Playa and Sagebrush sites. VWC is the volumetric water content, a is the surface albedo, k is the measured 50 mm thermal conductivity of the soil, C is the 50 mm volumetric heat capacity computed from $C = k/\alpha$ where α is the measured thermal diffusivity of the soil, $TI \equiv \sqrt{k * C}$ is the 50 mm thermal inertia of the soil, LAI is the leaf area index estimated from NASA's MODIS tool, and z_0 is the surface roughness

	Site	VWC	a	k (W m^{-1} K^{-1})	C (MJ K^{-1} m^{-3})	TI (J m^{-2} K^{-1} s$^{-1/2}$)	LAI	z_0 (mm)
Fall	Playa	0.30	0.31	0.90	2.2	1400	0	0.61
	Sagebrush	0.09	0.27	0.49	1.3	800	0.17	93
Spring	Playa	0.38	0.33	0.77	2.1	1270	0	0.11
	Sagebrush	0.13	0.24	0.72	1.7	1100	0.24	140

The surface roughness length (z_0) was estimated for both sites by considering wind speed profiles under near-neutral conditions. A least squares, linear regression of the wind speed (U) as a function of $\ln(z)$ was computed for each 5 min period. Regressions with R^2 values below 0.99 were removed. Next, the y-intercept of the regression was used to compute z_0 for each profile. Finally z_0 was estimated as the median value of z_0 from all profiles considered. As expected, $z_{0,Playa} \leq z_{0,Sagebrush}$, with $z_{0,Sagebrush}$ increasing in the spring, due to increased vegetation.

2.2 Instrumentation

At both sites, sonic anemometers and type-E thermocouples were used to capture turbulence data at multiple levels. The thermocouples used were 0.0127 mm in diameter with no radiation shield or active ventilation as the solar loading is expected to be negligible (Erell et al., 2005). The thermocouples were placed near the centre of sonic path for a spatial separation on the order of several tens of millimeters. The Playa site had six measurement levels between 0.5 and 26 m, while the Sagebrush site had five measurement levels between 0.5 and 20 m. Due to occasional instrumentation problems at the 26-m Playa tower, and to create consistency between sites, we only examine the five measurement heights between 0.5 and 20 m at both sites. Fast-response, open-path, infrared gas analyzers were positioned at 10 m at both sites, with a spatial distance of 60 mm from the sonic anemometer measurement volume, to measure the latent heat flux (H_L). At both sites, approximately 50 m to the west of the main towers, soil property sensors were buried at a depth of 50 mm to directly measure the thermal conductivity and diffusivity (α) of the soil. Finally, near the soil sensors, the four components of the radiation balance were measured on a sawhorse-type structure at 2 m above the surface. Site and sensor information is given in Table 2 and Fig. 2.

Table 2 Instrumentation deployed at the Playa and Sagebrush sites. Accuracy given as reported by the manufacturer. Tower locations refer to Fig. 2. u, v, and w are the streamwise, spanwise and vertical velocity components, respectively; T_s is the sonic derived temperature; H_2O is the mass density of H_2O ; P is atmospheric pressure; T is air temperature; RH is relative humidity; k is the soil thermal conductivity and α is the soil thermal diffusivity.

Instrument name	Variables measured	Accuracy	Sampling frequency (Hz)	Manufacturer	Tower Locations
CSAT3	u, v	$\pm$0.08 m s^{-1}	20	Campbell Sci.	A, B, C, D,
	w	$\pm$0.04 m s^{-1}			E, F, J
	T_s	n/a			
EC150	H_2O	n/a	20	Campbell Sci.	D, J
	P	$\pm$15 hPa			
RMY8100	u, v, w	$\pm$0.05 m s^{-1}	20	R.M. Young	G, H, I, K
	T_s	$\pm$ 2°C			
FW05	T	$\pm$0.07°C	20	Campbell Sci.	All
HMP45	T	$\pm$0.25°C	1	Vaisala	All
	RH	$\pm$ 2%			
TP01	k	$\pm$5%	1/600	Hukseflux	– 50 mm
	α	$\pm$20%			

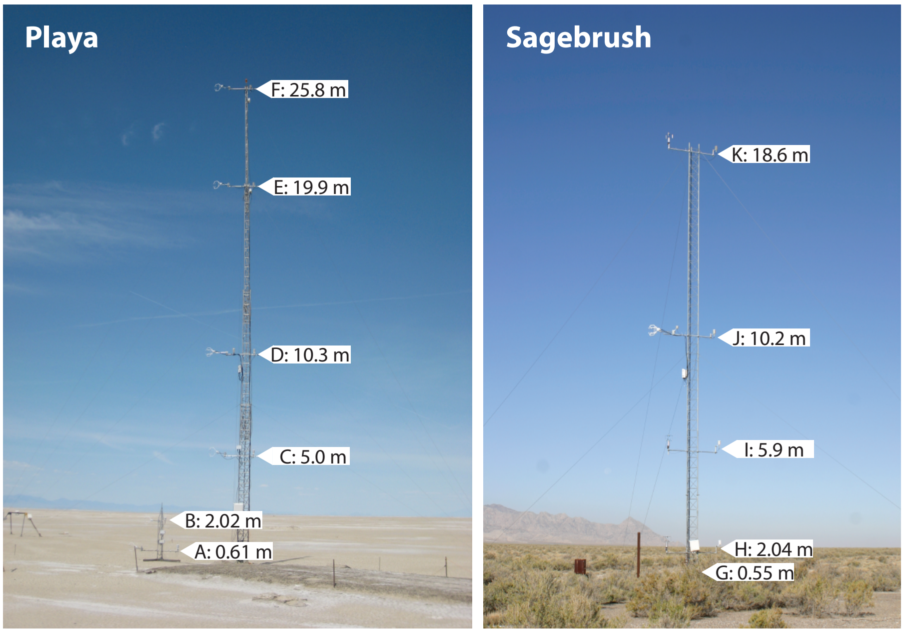

Fig. 2 Photographs looking north-west toward the Playa tower (left) and Sagebrush tower (right) with instrument heights imposed on the image. The northern portion of Granite Peak is visible behind the Sagebrush tower. Height labels refer to Table 2. For simplicity, tower heights are referred to as 0.5, 2, 5, 10, 20, and 26 m throughout this study. The 0.5 and 2 m Playa instrumentation is mounted on a smaller tower to the west of the main tower to minimize flow distortion. At both sites, the radiation balance and soil property measurements were made approximately 50 m to the west of the main tower.

2.3 Data Analysis

Data were analyzed with the Utah Turbulence in Environmental Studies processing and analysis code (UTESpac). Despiking and quality control were performed following Vickers and Mahrt (1997), planar fitting was applied following Wilczak et al. (2001) and density corrections were applied to the latent heat flux following Webb et al. (1980). Based on the previous work of Blay-Carreras et al. (2014) and ogive tests (Aubinet et al., 2012), 5-min averaging periods and linear detrending were chosen chosen as the best combination to isolate the turbulent motions from the rapidly evolving mean state through the EET. Finally, due to small spatial separations in the eddy-covariance systems, no spectral corrections were applied (Aubinet et al., 2012).

Temperature gradients were computed from the fine-wire thermocouples using finite difference techniques. A forward difference is used for the lowest level (Error $O(dz)$), a backward difference for the highest level (Error $O(dz)$), and a three-point difference (Error $O(dz^2)$), utilizing the analytical derivative of a Lagrange interpolating polynomial, for the middle levels (Chapra and Canale, 2010).

2.4 Transition Analysis

In order to study flux and gradient evolution through the EET, a relative time τ is defined as $\tau = t - t_{Rn=0}$ where t is time and $t_{Rn=0}$ is the first time period where the net radiation has become negative. τ_{flux} represents the relative time when the sensible heat flux (H) reverses direction and τ_{grad} represents the relative time when the potential temperature gradient ($\partial\overline{\theta}/\partial z$) reverses direction. The identification method of τ_{grad} and τ_{flux} differ one from the other. τ_{grad} is defined as the timestep following the last period where the gradient was negative. This is because the gradients at 5 m and above are weak with slightly positive and negative values before stabilization occurs. Once the stabilization has occurred, the gradients typically become persistently positive. Contrarily, τ_{flux} is identified by the first time period where the heat flux becomes negative. This is because the strongly positive fluxes transition into weakly negative fluxes with occasional positive values. The reversals were identified computationally with careful examination to ensure that the reversal is accurately captured. The mean gradient and heat flux behaviour is addressed in Sect. 3.3 and 3.4, respectively.

Next, we define a time lag, $t_{\text{lag}} = \tau_H - \tau_{\text{grad}}$ to quantify delays between the gradient and flux reversals. Therefore, $t_{\text{lag}} > 0$ indicates that the gradient reversal precedes the flux reversal (Fig. 5a, quadrant I) and $t_{\text{lag}} < 0$ indicates the flux reversal precedes the gradient reversal (Fig. 5b, quadrant III) which is the behaviour observed by Blay-Carreras et al. (2014).

Finally, we filter the data to eliminate transitions with incomplete data availability, excessive clouds, mean wind speeds above 10 m s^{-1} at 5 m, and non–monotonically decreasing temperatures through the late afternoon transition. We do this to limit our study to idealized, quiescent days with little synoptic forcing in an effort to focus on microscale phenomena. We are left with 8 transition periods at Playa and 13 at Sagebrush (Table 3).

3 Results and Discussion

3.1 Surface Fluxes

Fig. 3 shows the averaged net radiation (R_n), sensible heat flux (H), latent heat flux (H_L), potential temperature (θ), and wind speed for all days considered at both sites. The mean daytime R_n is appreciably higher at the Sagebrush site, consistent with the lower albedo, while the night time R_n magnitude is appreciably higher at the Playa site, consistent with the higher volumetric heat capacity and surface temperature (Fig. 5c). The formation and decay of sensible heat flux at Playa is much more gradual than that of Sagebrush. At the Sagebrush site, H reaches a maximum values of approximately 135 W m^{-2} that persists for several hours and then rapidly decays as R_n decreases. At the Playa site, H briefly builds to a maximum value of approximately 85 W m^{-2} and almost immediately begins to slowly decay. At Playa, the positive heat flux persists for approximatley an hour after net-radiative sunset while the reversal at Sagebrush typically occurs around 30 min after net-radiative sunset. Similar to the heat flux, the 10-m potential temperature at Playa increases and decreases much more gradually than Sagebrush, with a much smaller diurnal amplitude.

Given the arid nature of the region, the magnitude of H_L is quite small at both sites, H_L reaches a maximum of approximately 12 and 19 W m^{-2} at Playa and Sagebrush, respectively. Which yields a mean daytime Bowen ratio, defined as $\beta \equiv H/H_L$, of approximately 7 at both sites. Given the much higher soil moisture at Playa, this result is likely due to two things. First, the thin, smooth crust on the playa surface is effective at preventing moisture transport. Second, plant transpiration likely plays an important important role in the moisture budget at the Sagebrush site. Finally, though the sites are geographically close to one another, the smooth surface at the Playa site allows for significantly higher mean wind speeds.

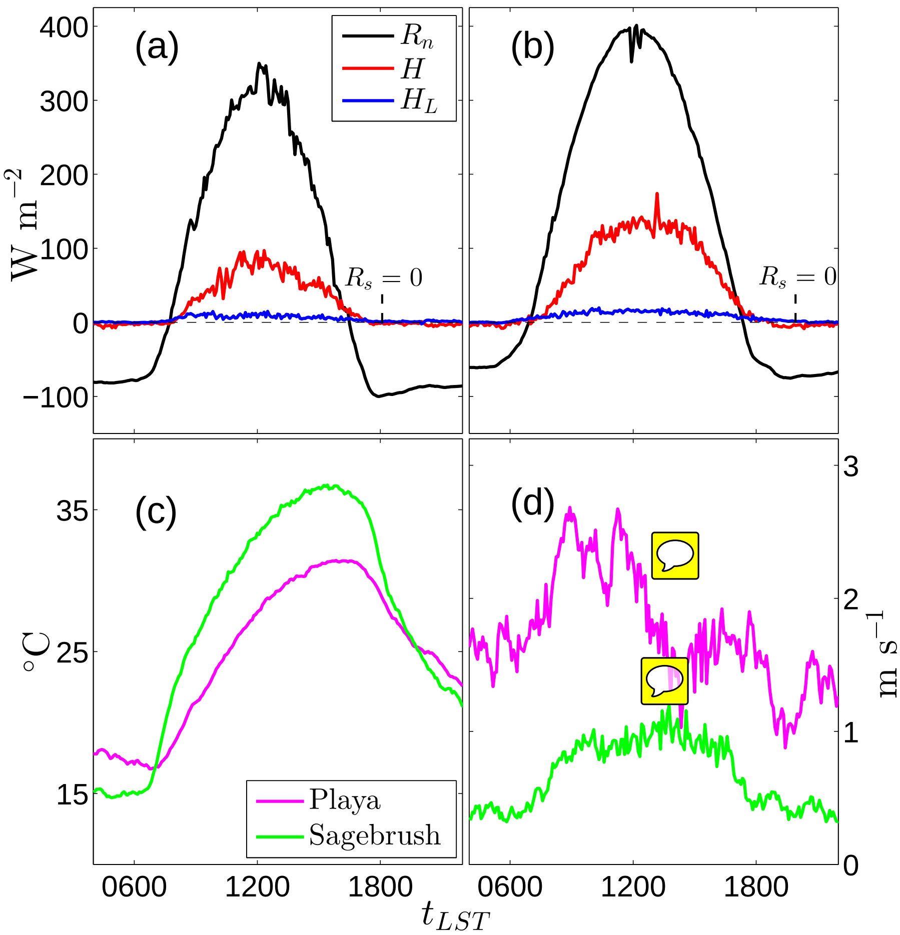

Fig. 3 Time series of the mean, 10-m variables for all days considered at both sites. Panel (**a**) and (**b**) give the sensible (H), latent (H_L) and net-radiative fluxes (R_n) at the Playa and Sagebrush sites, respectively. $R_s = 0$ indicates local solar-sunset. Panel (**c**) gives the mean potential temperature and panel (**d**) gives the mean wind speed.

3.2 Monin-Obukhov Scaling and Counter-Gradient behaviour

To better understand the scaling of fluxes and temperature profiles during the EET, the heat fluxes are plotted in the traditional Monin-Obukhov similarity theory (MOST) framework. Fig. 4 shows the non-dimensional temperature gradient (ϕ_h) as a function of stability (ζ). Where ϕ_h and ζ are defined as:

$$\phi_h(\zeta) = \frac{\kappa z}{\theta_*} \frac{\partial \overline{\theta}}{\partial z} \tag{1}$$

and

$$\zeta = \frac{z - d_0}{L}, \tag{2}$$

where $\kappa = 0.4$ is the von Kármán constant, $\overline{\theta}$ is the mean potential temperature, $\theta_* = -\overline{w'\theta_0'}/u_*$ is the scaling temperature, z is the height above the surface, d_0 is the displacement height, which is assumed to be zero at both sites, and L is the Obukhov length, defined as:

$$L = \frac{-u_*^3}{\kappa \frac{g}{\overline{\theta_0}} \overline{w'\theta_0'}}, \tag{3}$$

where u_* is the friction velocity, $\overline{\theta_0}$ is the mean potential temperature of air at the surface, g is acceleration due to gravity and $\overline{w'\theta_0'}$ is the surface kinematic heat flux.

For moderately unstable conditions ($-2.5 < \zeta \lesssim -0.2$), both sites scale quite well and ϕ_h is only slightly larger than the empirical formulation recommended by Dyer and Hicks (1970), which is indicated by the dashed black line. For moderately stable conditions ($0.2 \lesssim \zeta < 1$), the scatter is large at both sites. A trend is visible but it is less well defined and the slope is much steeper than the Dyer formulation, suggesting that an alternate formulation of ϕ_h may be more appropriate. Under near-neutral conditions ($-0.1 \lesssim \zeta \lesssim 0.1$), an asymptotic behaviour with large positive and negative values is observed. This behaviour is due to H being in the denominator of ϕ_h via θ_*(Eq. 1). The negative values of ϕ_h indicate that the local heat flux is counter-gradient. Theoretically, this regime corresponds to the classical neutrally stratified surface layer where θ_* is no longer a relevant scaling variable. However, neutral scaling does not apply during this transition either. Non-local effects become important and the local temperature gradient is a poor indicator of the local heat flux.

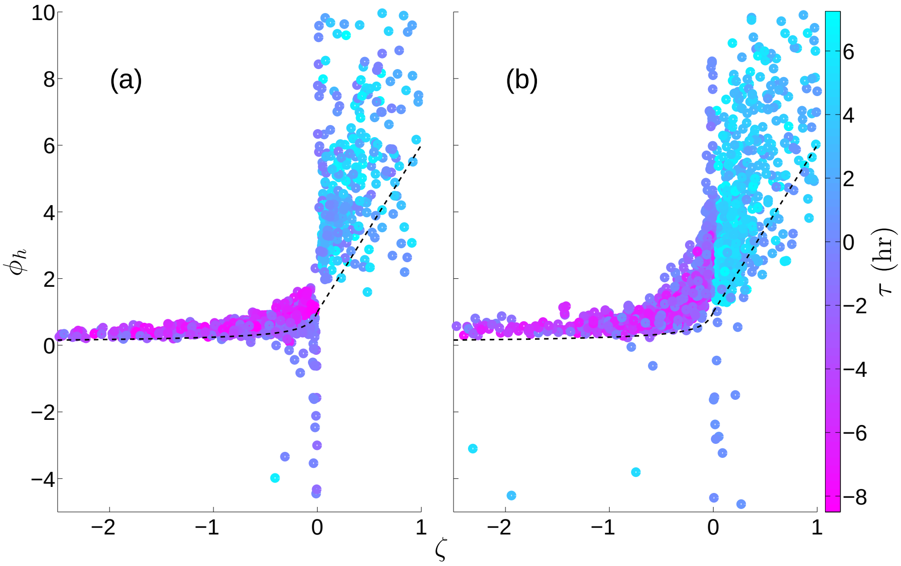

Fig. 4 The non-dimensional temperature gradient (ϕ_h) plotted as a function of stability (ζ) at 2 m for Playa **(a)** and Sagebrush **(b)**. The markers are experimental data from 8.5 hours before net-radiative sunset ($\tau = 0$) to 7 hours after. The dashed line is the empirical form of ϕ_h recommended by Dyer and Hicks (1970).

To explore the counter-gradient phenomena, quadrant analysis of the kinematic sensible heat flux ($\overline{w'\theta'}$) and potential temperature gradient ($\partial\overline{\theta}/\partial z$) at 2 m is used (Fig. 5). Physically, Quadrant II corresponds to typical afternoon conditions where the heat flux is positive and $\partial\overline{\theta}/\partial z$ is negative. The curve in Quadrant II at Playa is relatively linear and steep with minimal fluctuations, indicating reasonable flux-gradient behaviour. At Sagebrush, the flux weakens substantially while the unstable temperature gradient remains relatively strong, indicating that the turbulent diffusivity, defined as $K_h = \overline{w'\theta'}/(\partial\overline{\theta}/\partial z)$, is relatively small and non-linear. Quadrant IV corresponds to typical nighttime conditions where the heat flux is negative and the gradient is positive. At the Sagebrush site, a maximum negative heat flux occurs for $\partial\overline{\theta}/\partial z \approx 0.2$ indicating a maximization of mixing efficiency as the surface layer stabilizes (Caughey et al., 1979). There is no clear evidence of this at the Playa site. Quadrants I and III correspond to counter-gradient heat fluxes. In Quadrant I, H remains positive after the gradient has changed sign ($t_{\mathrm{lag}} > 0$). This behaviour describes all counter-gradient periods at the Playa site. In Quadrant III, the gradient remains negative after H has changed sign ($t_{\mathrm{lag}} < 0$). This behaviour describes nearly all transitional, counter-gradient situations at the 2-m Sagebrush site (note that some Quadrant I behaviour occurs at Sagebrush long after transition) and is consistent with the observations of Blay-Carreras et al. (2014).

Table 3 contains τ_{grad} , τ_{flux} and t_{lag} for all days considered at 2 m for the Playa and Sagebrush sites. τ_{grad} shows some similarity between sites with much higher variability at the Playa site. τ_{flux} is typically smaller for the Sagebrush site with higher variability at Playa. t_{lag} is fairly consistent for both sites. $|t_{\mathrm{lag}}|$ is typically between 5

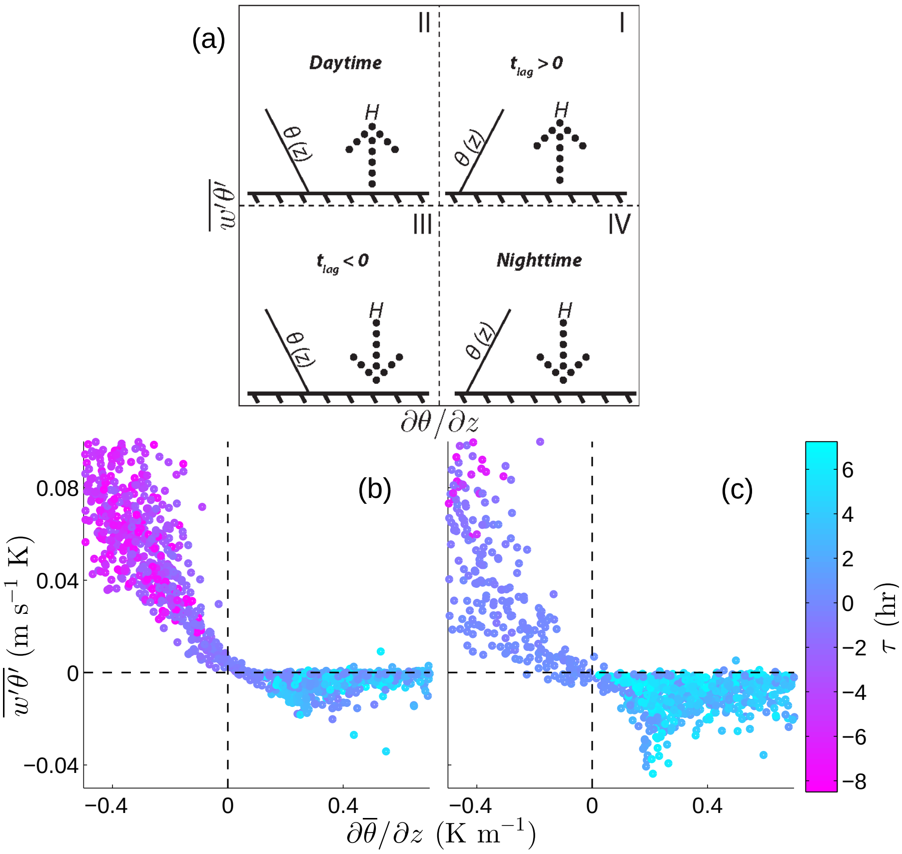

Fig. 5 Quadrant analysis of the kinematic sensible heat flux and potential temperature gradient. **(a)** shows the qualitative behaviour of each quadrant. Quadrants II and IV correspond to daytime and nighttime conditions, respectively. Quadrants I and III correspond to counter-gradient heat fluxes. In Quadrant I the gradient reversal precedes the flux reversal; in Quadrant III the flux reversal precedes the gradient reversal. The 2-m Playa site **(b)** is dominated by $t_{\mathrm{lag}} > 0$ while the 2-m Sagebrush site **(c)** is dominated by $t_{\mathrm{lag}} < 0$. Data is colored by τ.

and 20 minutes for both sites with negative values associated with Sagebrush (Quadrant III from Fig. 5) and positive values associated with Playa (Quadrant I). The large variability in τ_{grad} and τ_{flux} with the accompanying small variability associated with t_{lag} at Playa indicates that the counter-gradient behaviour is fairly consistent. That is, regardless of when transition occurs, if τ_{grad} is known, τ_{flux} may be inferred and vice versa. This is also the case at Sagebrush, but in addition, τ_{flux}, τ_{grad} and t_{lag} may be estimated from only $t_{Rn=0}$.

Table 3 Counter-gradient timing variables for 2 m at Playa and Sagebrush. $t_{R_n=0}$ is the local net-radiative sunset in local standard time (LST), τ_{grad} is the time of the local temperature gradient reversal relative to $t_{R_n=0}$, τ_{flux} is the relative time of the heat flux reversal, and t_{lag} is the counter-gradient duration computed by subtracting τ_{grad} from τ_{flux}.

Site	Date	$t_{R_n=0}$ (LST)	τ_{grad} (min)	τ_{flux} (min)	t_{lag} (min)
Playa	7 Oct ’12	1640	45	65	20
	14 Oct ’12	1650	35	40	5
	15 Oct ’12	1650	10	20	10
	17 Oct ’12	1630	60	70	10
	18 Oct ’12	1630	55	70	15
	19 Oct ’12	1635	10	20	10
	20 Oct ’12	1640	–25	0	25
	21 Oct ’12	1600	45	70	25
Sagebrush	28 Sept ’12	1710	40	30	–10
	29 Sept ’12	1715	20	15	–5
	1 Oct ’12	1700	45	30	–15
	2 Oct ’12	1710	25	20	–5
	3 Oct ’12	1710	30	20	–10
	4 Oct ’12	1710	30	25	–5
	6 Oct ’12	1700	45	35	–10
	7 Oct ’12	1700	45	40	–5
	8 Oct ’12	1700	25	35	10
	9 Oct ’12	1645	20	15	–5
	12 May ’13	1835	20	15	–5
	24 May ’13	1835	30	20	–10
	30 May ’13	1850	20	20	0

Box plots are used to illustrate τ_{grad}, τ_{flux} and t_{lag} for all heights across all days considered (Fig. 6 - 8). First considering τ_{grad}, the variability is smaller at Sagebrush, but the median time of gradient reversal is approximately constant between sites for a given height. Furthermore, gradient reversal is a top-down phenomena with a slope of

$$\frac{\partial \tau_{\mathrm{grad}}}{\partial z} \approx -4 \text{ min m}^{-1} \tag{4}$$

at both sites, indicating that within the context of this study, gradient reversal is top-down and site independent.

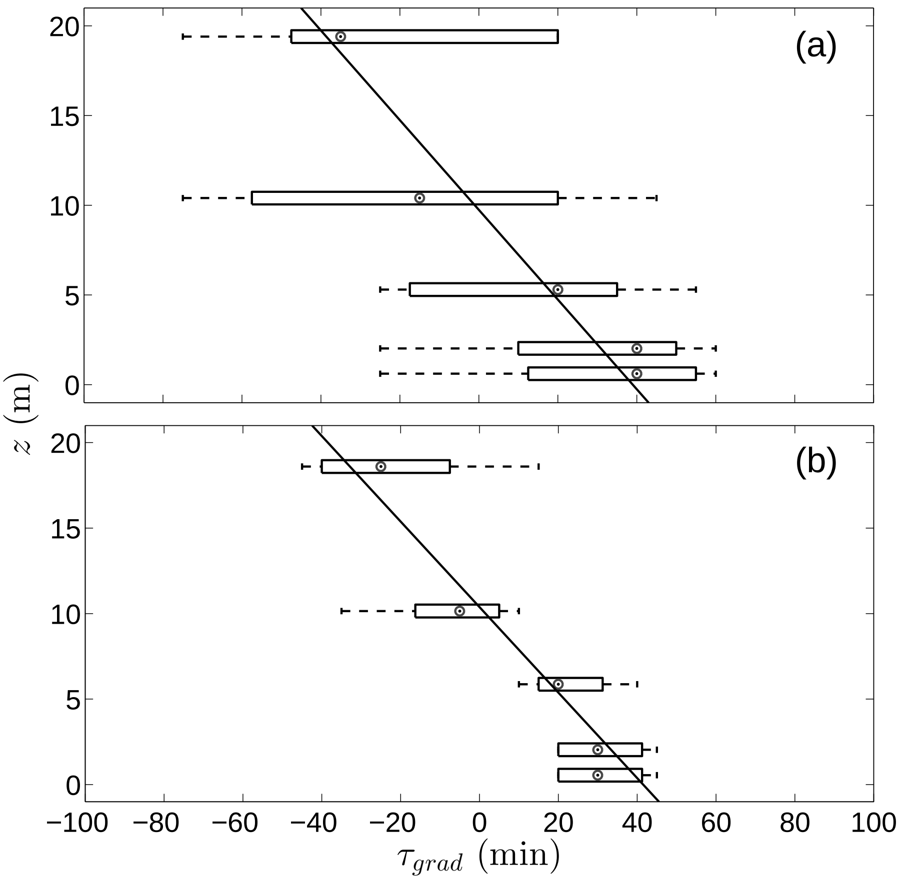

Fig. 6 Box plots of gradient reversal time τ_{grad} for Playa **(a)** and Sagebrush **(b)**. The target within the box represents the median value, the left and right walls of the box represent the first and third quartiles and the whiskers represent data that fall within 1.5 times the interquartile range (IQR) of the nearest box wall. Any markers beyond the whiskers represent individual outliers. The solid line is a linear fit of the median values based on Eq. 4.

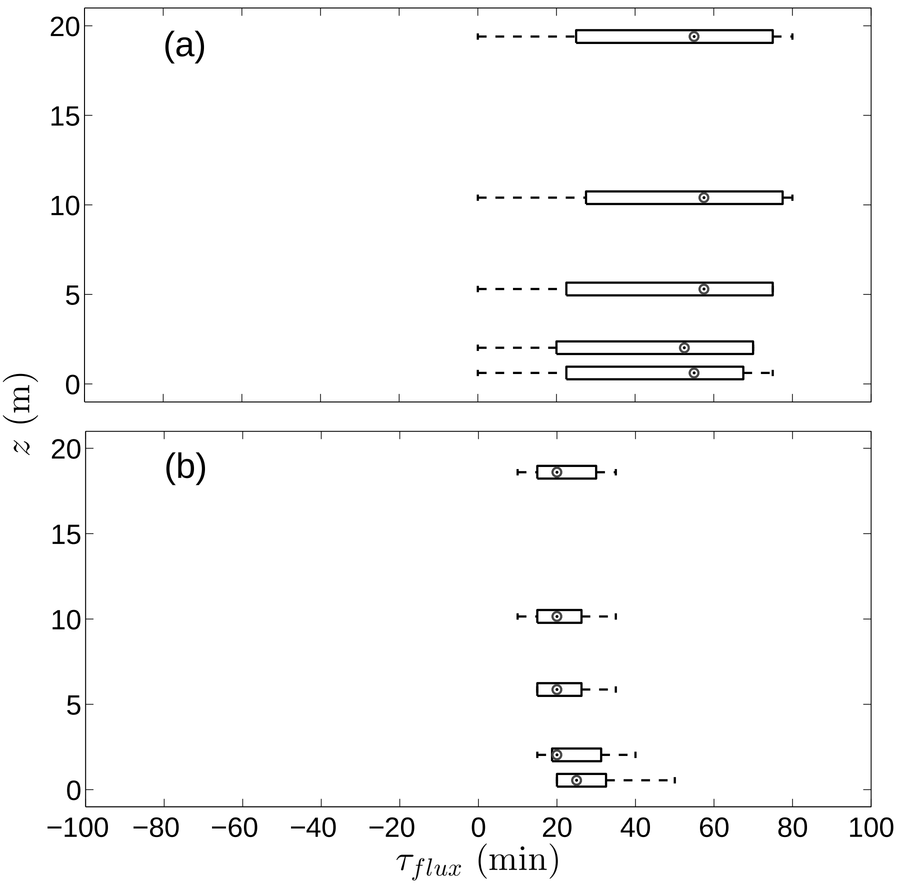

Fig. 7 Box plots of the heat flux reversal time τ_{flux} for Playa **(a)** and Sagebrush **(b)**. The target within the box represents the median value, the left and right walls of the box represent the first and third quartiles and the whiskers represent data that fall within 1.5 times the interquartile range (IQR) of the nearest box wall. Any markers beyond the whiskers represent individual outliers. The flux reversal occurs nearly simultaneously at both sites, with the Playa reversal occurring later than that of Sagebrush.

Next, τ_{flux} (Fig. 7) is considered. Again, the variability at Playa is quite large but invariant across all heights. When individual days are considered (not shown), the flux reversal occurs nearly simultaneously at all heights. Thus, the variability in Fig 7a is predominantly due to the relatively weak correlation between the net-radiative sunset and flux reversal. The median flux reversal at Playa typically occurs 30 - 40 minutes later than at Sagebrush. Unlike the gradient reversal, the flux reversal is strongly site-dependent but independent of height. This is counter to what Caughey and Kaimal (1977) reported, where they observed the flux to change sign from top to bottom over a larger height range than measured in the present experiment. Given this information, we hypothesize that $t_{\text{lag}}(\Delta z)$ may be approximated near the surface with only t_{lag} at a single height by

$$t_{\text{lag}}(\Delta z) \approx -\frac{\partial \tau_{\text{grad}}}{\partial z}\Delta z - (\tau_{grad,z} - \tau_{flux,z}) \tag{5}$$

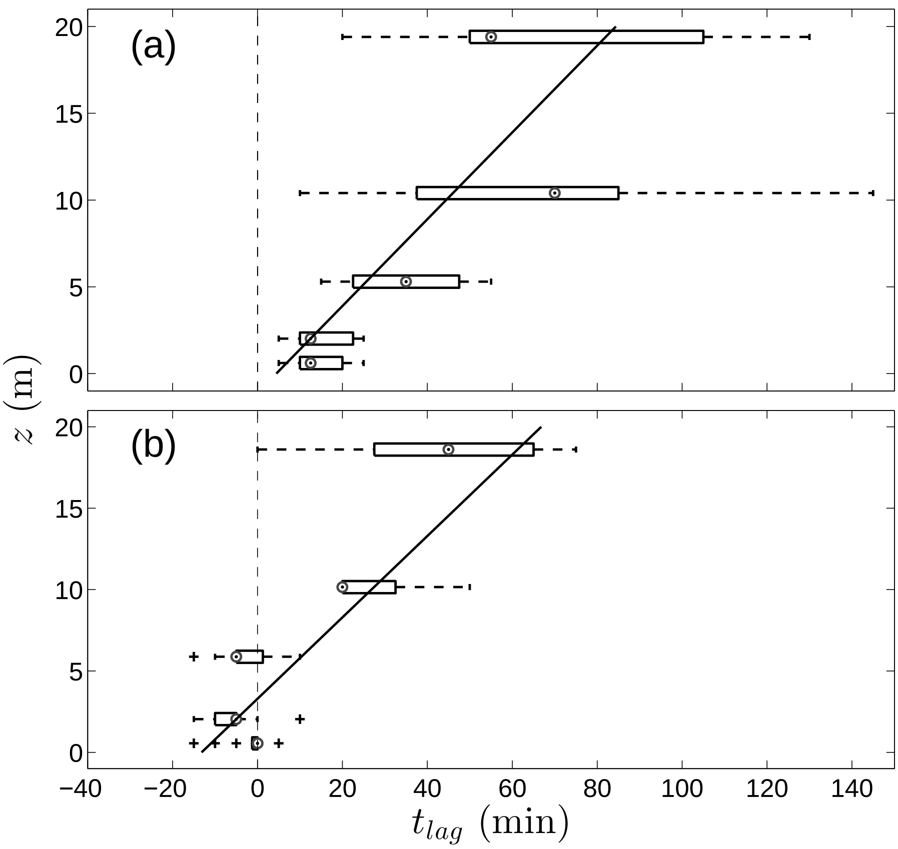

Fig. 8 Box plots of t_{lag} for Playa **(a)** and Sagebrush **(b)**. The solid line is calculated from Eq. 4 and 5 with the 2-m values of τ_{flux} and τ_{grad}. The 2-m $|t_{\text{lag}}|$ is smaller than expected and is likely influenced by canopy effects.

Fig. 8 shows $t_{\mathrm{lag}}(z)$ with the solid line representing Eq. 4 and 5, calculated from τ_{grad} and τ_{flux} at 2 m. The uncertainty in t_{lag} grows with height at both sites, due to the weak temperature gradients aloft, but Eq. 5 generally captures the trend and typically falls within the interquartile range (IQR) of the box plots (marked by the limits of the the box).

3.3 Temperature Gradient Evolution and Flux Divergence

To understand the differing counter-gradient behaviour at the Playa and Sagebrush sites, the temperature gradient and heat flux evolution are considered independently. First, the temperature gradient evolution is discussed followed by the heat flux evolution in Sect. 3.4.

The mean temperature gradient evolution is shown for both sites in Fig. 9. As expected, the relative strength of the gradients are much stronger at Sagebrush for both before and after net-radiative sunset. The gradients at 10 and 20 m at Sagebrush are quasi-neutral and slowly begin to stabilize slightly before $\tau = 0$. This is also the case at the Playa site, however at Playa, the 5-m gradient is also quasi-neutral before stabilization occurs. At both sites, the weak gradients aloft cross zero before the stronger, near-surface gradients at 0.5 and 2 m. Additionally, there is never a period where all of the gradients are near-neutral. In fact, at both sites there appears to be a brief period where all of the gradients are approximately equal and weakly stable. This abrupt transition through zero supports the modeling work of Jiménez et al. (2012) and observations of Acevedo and Fitzjarrald (2001) where the transition through neutral stratification happens abruptly.

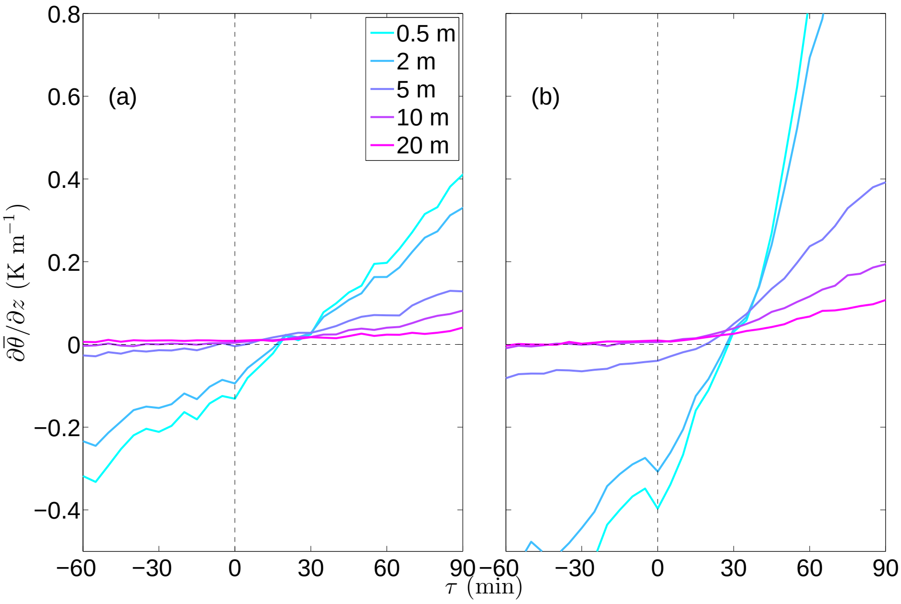

Fig. 9 Time series of the mean potential temperature gradient for all heights at the Playa (**a**) and Sagebrush sites (**b**). $\tau = 0$ is the net-radiative sunset. The top-down gradient reversal times are $\tau_{\text{grad,Playa}}(z = 0.5, 2, 5, 10, 20\text{ m}) = 15$, 15, 0, –40, –195 min and $\tau_{\text{grad,Sagebrush}}(z = 0.5, 2, 5, 10, 20\text{ m}) = 25$, 25, 15, –20, –40 min.

The weak gradients aloft help to explain why the gradient reversal occurs from the top down. Temperature tendency profiles are shown in Fig. 10. Once again, the magnitude of the cooling at Sagebrush is much larger than that at Playa. At both sites the cooling is largest and initiated near the ground. The stabilization in the layer is proportional to the slope of the temperature tendency profile. Therefore, while stabilization is occurring most rapidly near the surface, the very weak gradients aloft are able to change sign with a very small amount of stabilization, resulting in the observed top-down behavior.

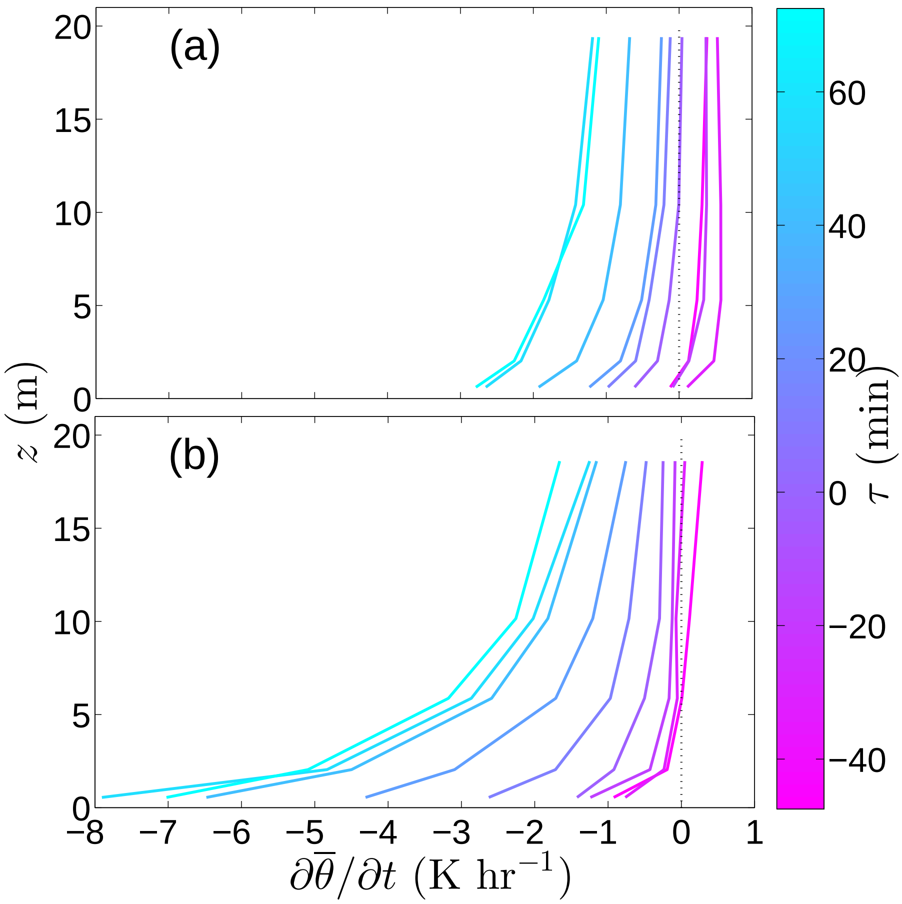

Fig. 10 Profiles of $\partial\overline{\theta}/\partial t$ at Playa **(a)** and Sagebrush **(b)**. To the right of the dashed line, heating is occurring and to the left of the dashed line, cooling is. A 15 minute bin-average was applied to the profiles.

To understand the mechanism of the cooling, the simplified temperature tendency equation is considered (e.g. Acevedo and Fitzjarrald, 2001):

$$\underbrace{\frac{\partial\overline{\theta}}{\partial t}}_{\mathrm{I}} = \underbrace{-\frac{\partial\overline{w'\theta'}}{\partial z}}_{\mathrm{II}} \underbrace{+ADV_{\theta} - \frac{\partial R_n}{\partial z}}_{\mathrm{III}} \tag{6}$$

where term I is the rate of change in temperature, II is the sensible heat flux divergence, and III, which is computed as the residual, is the sum of all advective effects (ADV_{θ}) and the radiative flux divergence ($\frac{\partial R_n}{\partial z}$). It is expected that early in the EET, temperature advection will be relatively small and gradually increase in importance as the size of the mixing eddies decreases and surface heterogeneities are amplified (Acevedo and Fitzjarrald, 2001, 2003).

The terms of Eq. 6 are plotted for 5 m at both sites in Fig. 11. When terms II or III are greater than zero, ~~the term is~~ warming the layer; when they are less than zero,

~~the term is~~ cooling the layer. At the Playa site, the heat flux divergence begins to cool the layer at approximately the same time term I becomes negative. That is, there is a heat flux convergence in the layer until the layer begins to cool (I$<$ 0), at which point the convergence gradually shifts to a divergence. The maximum cooling rate is then in approximate agreement with the largest heat flux divergence, in agreement with the findings of Acevedo and Fitzjarrald (2001). Term I shows no clear minimum (or maximum cooling rate) over the time range shown. This is due to the ensembled nature of the data. When individual days are considered (not shown), often, there is an abrupt decrease in the time series of T followed by an inflection point, indicating the mechanical turbulence has decayed (Fitzjarrald and Lala, 1989).

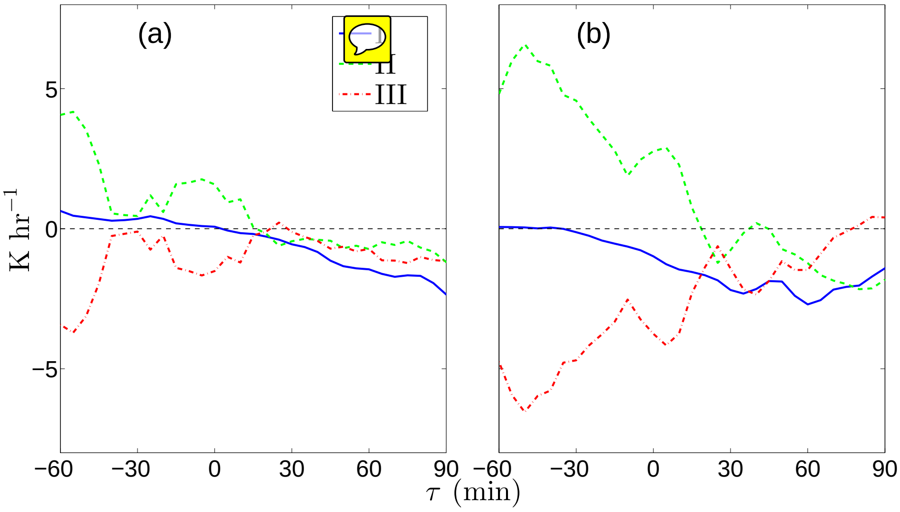

Fig. 11 Terms of the simplified temperature tendency equation (Eq. 6) for 5 m at the Playa (**a**) and Sagebrush (**b**) sites. Term I is the local time change of temperature, term II is the sensible heat flux divergence and term III is the cumulative effect of advection and radiative flux divergence. Term III is computed as a residual. A 25 min running average is used to smooth the ensembled data.

At the Sagebrush site, the magnitudes of term I and II are much larger. This is due to the stronger heat fluxes and temperature gradients at Sabebrush. The air begins to cool (term I) significantly before the heat flux convergence (term II) shifts to a divergence, with much of the cooling occurring in the presence of a weak sensible heat flux convergence. This is counter to the findings of Acevedo and Fitzjarrald (2001), where the maximum cooling rate was found to coincide with the maximum heat flux divergence. Considering the relative homogeneity of both sites, and presumably weak advection, it appears that radiative flux divergence becomes important earlier in the EET than previously thought (Acevedo and Fitzjarrald, 2001) and should not be neglected in models. When other tower heights are considered (not shown), the observed behaviour is very similar to the 5-m level, the only difference being that the relative magnitude of the terms decreases with height.

3.4 Heat Flux Evolution

Here, the sensible heat flux evolution is considered. The mean sensible heat flux evolution is shown in Fig. 12. At the Playa site, the decay is gradual with a small amount of variability (heat flux convergence) between levels. The heat flux at all levels reverses direction at approximately the same time and a weak heat flux divergence gradually develops through the evening transition. At the Sagebrush site, the decay is much more abrupt, with a large heat flux convergence occurring in the lower levels. The levels above 0.5 m reverse direction at approximately the same time with the 0.5-m flux crossing 5–10 minutes later. This is likely due to shielding from the surrounding vegetation. Later in the evening transition, the negative fluxes at Sagebrush become stronger than those observed at Playa with a sensible heat flux divergence developing around $\tau = 45$ min.

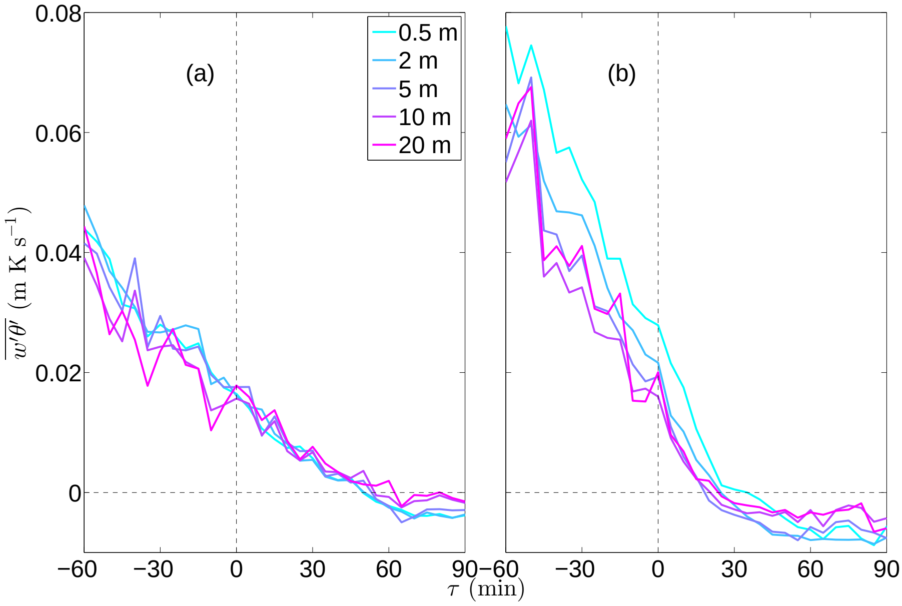

Fig. 12 Time series of the ensemble sensible heat flux for all heights at the Playa (**a**) and Sagebrush sites (**b**).

Similar to the temperature gradient evolution, the heat flux evolution is discussed in terms of its simplified tendency equation. Here we used the simplified budget for horizontally homogeneous terrain from Wyngaard et al. (1972):

$$\underbrace{\frac{\partial \overline{w'\theta'}}{\partial t}}_{\mathrm{I}} = \underbrace{-\overline{w'^2}\frac{\partial \overline{\theta}}{\partial z}}_{\mathrm{II}} \underbrace{-\frac{\partial \left(\overline{w'^2\theta'}\right)}{\partial z}}_{\mathrm{III}} \underbrace{+\frac{g}{\overline{\theta}}\overline{\theta'^2}}_{\mathrm{IV}} \underbrace{-\frac{1}{\rho}\overline{\theta'\frac{\partial p'}{\partial z}}}_{\mathrm{V}} \tag{7}$$

where term I is local storage, II is gradient production, III is the turbulent transport, IV is buoyant production and V is the pressure destruction. Subsidence, advection, and molecular dissipation are assumed to be small. Terms I – IV are computed directly and term V is computed as a residual. The mean terms at 5 m are shown in Fig. 13. Again, the relative magnitude of the terms is much larger at the Sagebrush site. This is due to the stonger temperature gradients and increased surface roughness at Sagebrush. For $\tau < 0$, the buoyant production term (IV) is more important than the gradient production (II) at the Playa site, while the opposite is true at the Sagebrush site. By definition, IV is always positive, meaning that IV will always delay the decay of the sensible heat flux. Term II has the opposite sign of the local gradient, meaning that II will force the heat flux to decay in consonance with the local gradient reversal. The turbulent transport (III) is relatively noisy but insignificant at both sites. Term V, which is computed as a residual, is quite large at the Sagebrush site and becomes a source of sensible heat flux later into the EET, indicating that advection is likely important during this process.

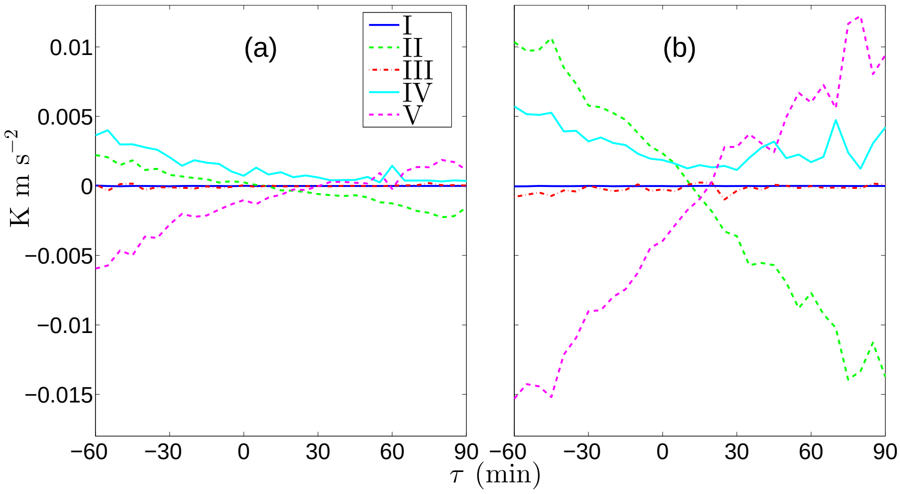

Fig. 13 Terms in the flux tendency equation (Eq. 7) ~~plotted~~ at 5 m for the Playa (**a**) and Sagebrush (**b**) sites. Term I is local storage of sensible heat, II is gradient production, III is the turbulent transport, IV is buoyant production and V is the pressure destruction.

We hypothesize that the relative importance of terms II and IV leading up to the flux reversal play a fundamental role in the observed counter-gradient behaviour. When buoyant production (IV) is substantially larger than gradient production (II), we expect that the decay will be delayed and the positive heat flux will persist in the presence of a stable temperature gradient ($t_{\mathrm{lag}} > 0$). Conversely, when term II is more important than term IV we expect the behaviour observed by Blay-Carreras et al. (2014). That is the heat flux reversal occurs in the presence of a weakly unstable temperature gradient ($t_{\mathrm{lag}} < 0$). The reason for the flux reversal occurring before the gradient reversal, rather than at the same time is related to the inverse Rayleigh-Bernard problem, where the weak, unstable temperature gradients become insufficient to overcome viscous forces. The behaviour is discussed at length in Blay-Carreras et al. (2014).

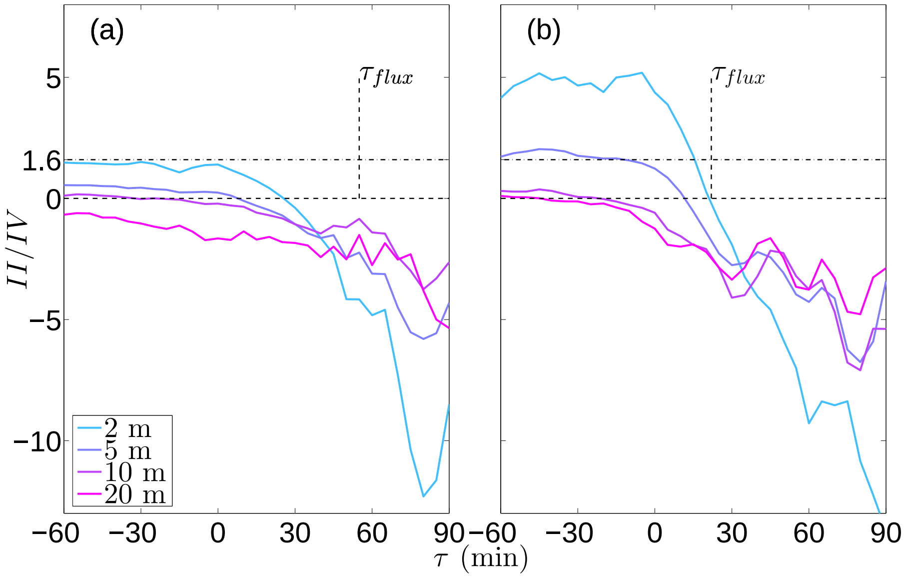

Fig. 14 Time series of the ratios of gradient (II) to buoyant (IV) production from the heat flux tendency equation (Eq. 7) for the Playa (**a**) and Sagebrush (**b**) sites. A 15 minute running averages is applied to smooth the data and the heat flux reversal is marked by $\tau_{\rm flux}$ at both sites. The horizontal line at II/IV$= 1.6$ is a critical ratio. For pre-transition ratios above this, the counter-gradient flux occurs when the flux reversal precedes the gradient reversal ($\tau_{\rm lag} < 0$). For pre-transition ratios below 1.6, the counter-gradient flux occurs when the gradient reversal precedes the flux reversal ($\tau_{\rm lag} > 0$). The counter-gradient duration is proportional to the difference between the pre-transition ratio and 1.6.

To test this hypothesis, the ratio II/IV is plotted for all heights in Fig. 14. For a prolonged period before flux reversal occurs there is a period at all locations where the ratio II/IV is approximately constant. This pre-transition ratio (II/IV$|_{PT}$) determines the type and duration of the counter-gradient behavior, where II/IV$|_{PT} \approx 1.6$ is a critical value. For II/IV$|_{PT} > 1.6$, $t_{\rm lag}$ is less than zero (the behaviour observed by Blay-Carreras et al. (2014)). For II/IV$|_{PT} < 1.6$, $t_{\rm lag} > 0$. The counter-gradient duration is proportional to the magnitude of the difference between the observed pre-transition ratio and 1.6. That is, the further II/IV$|_{PT}$ deviates from 1.6, the larger $|t_{\rm lag}|$ becomes. This is apparent for 2 m at the Playa site and 5 m at the Sagebrush site. Both locations display small magnitudes of $t_{\rm lag}$ with the Playa 2-m location being weakly positive and the 5-m Sagebrush location being weakly negative. Table 4 gives II/IV$|_{PT}$ as well as the observed mean lag time $\overline{t_{\rm lag}}$ for all heights at both sites.

Table 4 Pre-transition ratios of the gradient (term II) to buoyant production (term IV) terms in the heat flux tendency eqaution (Eq. 7) at all heights for Playa and Sagebrush, where subscript PT denotes pre-transition. The ratio $\mathrm{II/IV}|_{PT}$ is a critical value that determines whether t_{lag} will be positive or negative.

Site	z (m)	$\mathrm{II/IV}\|_{PT}$	$\overline{t_{\mathrm{lag}}}$ (min)
Playa	2	1.5	15
	5	0.5	35
	10	0.1	68
	20	–1	71
Sagebrush	2	5	-6
	5	1.7	-2
	10	0.4	28
	20	0.1	44

4 Conclusions

Data from the MATERHORN Program were used to study near-surface, sensible heat flux and temperature gradient profiles through the early evening transition (EET) over two contrasting sites. The main conclusions are:

1. During the EET, there is typically a lag between the time of local temperature gradient reversal and local heat flux reversal, leading to a period of counter-gradient heat flux. The gradient reversal may precede the flux reversal ($t_{\mathrm{lag}} > 0$) and vice-versa ($t_{\mathrm{lag}} < 0$). The duration and type of counter-gradient behavior is strongly height and site dependent.
2. The gradient reversal propagates from the top down at a rate of approximately 4 min m^{-1} and displays site independence (Fig 6). The top-down behaviour is due to very weak gradients aloft that reverse with a small amount of stabilization (Fig. 9 and 10).
3. The heat flux reversal occurs nearly simultaneously at all heights but displays site dependence, with the reversal at the Playa site occurring later than the Sagebrush site.
4. Based on the top-down gradient reversal and simultaneous flux reversal, the counter-gradient behavior can be estimated as a function of height if the gradient and flux reversal are known at a single location (Eq. 5).
5. Radiative flux divergence may become important earlier in the EET than previously thought. The radiative cooling behaviour is particularly at the Sagebrush site (Fig. 11).
6. The type and duration of the counter-gradient behaviour can be predicted by comparing the relative strength of the gradient production to buoyant production terms in the heat flux tendency equations. There is a critical ratio of approximately 1.6. If the ratio is greater than 1.6, the flux reversal is likely to precede the gradient reversal ($t_{\mathrm{lag}} < 0$). If the ratio falls below 1.6, the opposite is true. The counter-gradient duration is proportional to the difference between the ratio and 1.6.
7. Future work should include a similar analysis over differing subsurface and surface types to verify the general applicability of the results.

Acknowledgements This research was funded by the Office of Naval Research Award #$N00014-11-1-0709$, Mountain Terrain Atmospheric Modeling and Observations (MATERHORN) Program. The authors would like to thank Michael Carston, Paul Broderick, Dr. Dragan Zajic and John Pace from the Dugway Proving Ground whose contributions were critical to the success of the field measurements. We are also extremely grateful for all of the help in the field and scientific insight provided by the MATERHORN team, especially Prof. H.J.S. Fernando. Finally, we would like to thank the reviewers of the manuscript. Their comments and suggestions were invaluable to the improvement of the study.

References

Acevedo OC, Fitzjarrald DR (2001) The early evening surface-layer transition: Temporal and spatial variability. J Atmos Sci 58:2650–2667

Acevedo OC, Fitzjarrald DR (2003) In the core of the night – Effects of intermittent mixing on a horizontally heterogeneous surface. Boundary-Layer Meteorol 106:1–33

Angevine WM (2007) Transitional, entraining, cloudy, and coastal boundary layers. Acta Geophys 56:2–20

Aubinet M, Vesala T, Papale D (2012) Eddy Covariance - A Practical Guide to Measurement and Data Analysis — Springer. Springer, Dordrecht, Heidelberg, London, New York, p 438

Blay-Carreras E, Pardyjak ER, Pino D, Alexander DC, Lohou F, Lothon M (2014) Countergradient heat flux observations during the evening transition period. Atmos Chem Phys 14:9077–9085

Brown AR, Cederwall RTR, Chlond A, Duynkerke P, Golaz JC, Khairoutdinov M, Lewellen DC, Lock AP, MacVean MK, Moeng CH, Neggers RAJ, Siebesma AP, Stevens B (2002) Large-eddy simulation of the diurnal cycle of shallow cumulus convection over land. Q J R Meteorol Soc 128:1075–1093

Caughey SJ, Kaimal JC (1977) Vertical heat flux in the convective boundary layer. Q J R Meteorol Soc 103:811–815

Caughey SJ, Wyngaard JC, Kaimal JC (1979) Turbulence in the Evolving Stable Boundary Layer. J Atmos Sci 36:1041–1052

Chapra S, Canale R (2010) Numerical Methods for Engineers. 6th edn, McGraw-Hill Higher Education, Boston, p 658

Cole GS, Fernando HJS (1998) Some aspects of the decay of convective turbulence. Fluid Dyn Res 23:161–176

Comte-Bellot G, Corrsin S (1971) Simple Eulerian time correlation of full-and narrow-band velocity signals in grid-generated, isotropic turbulence. J Fluid Mech 48:273–337

Deardorff J (1970) Convective velocity and temperature scales for the unstable planetary boundary layer and for Rayleigh convection. J Atmos Sci 27:1211–1213

Dyer AJ, Hicks BB (1970) Flux-gradient relationships in the constant flux layer. Q J R Meteorol Soc 96:715–721

Edwards JM, Beare RJ, Lapworth AJ (2006) Simulation of the observed evening transition and nocturnal boundary layers: Single-column modelling. Q J R Meteorol Soc 132:61–80

Emrick V, Hill A (1999) Classification of Great Basin plant communities occuring on Dugway Proving Ground, Utah. Elus Doc 64

Erell E, Leal V, Maldonado E (2005) Measurement of air temperature in the presence of a large radiant flux: An assessment of passively ventilated thermometer screens. Boundary-Layer Meteorol 114:205–231

Fedorovich E, Nieuwstadt FTM, Kaiser R (2001) Numerical and laboratory study of horizontally evolving convective boundary layer. Part II: Effects of elevated wind shear and surface roughness. J Atmos Sci 58:546–560

Fitzjarrald DR, Lala GG (1989) Hudson valley fog environments. J Appl Meteorol 28:1303–1328

Google Earth (2013) Dugway Proving Ground, UT, USA

Goulart AG, Bodmann BEJ, de Vilhena MTMB, Soares PMM, Moreira DM (2010) On the time evolution of the turbulent kinetic knergy spectrum for decaying turbulence in the convective boundary layer. Boundary-Layer Meteorol 138:61–75

Grant ALM (1997) An observational study of the evening transition boundary-layer. Q J R Meteorol Soc 123:657–677

Grimsdell AW, Angevine WM (2002) Observations of the afternoon transition of the convective boundary layer. J Appl Meteorol 41:3–11

Jiménez Pa, Dudhia J, González-Rouco JF, Navarro J, Montávez JP, García-Bustamante E (2012) A revised scheme for the WRF surface layer formulation. Mon Weather Rev 140:898–918

Kang HS, Chester S, Meneveau C (2003) Decaying turbulence in an active-grid-generated flow and comparisons with large-eddy simulation. J Fluid Mech 480:129–160

Kumar V, Kleissl J, Meneveau C, Parlange MB (2006) Large-eddy simulation of a diurnal cycle of the atmospheric boundary layer: Atmospheric stability and scaling issues. Water Resour Res 42:1–18

Kumar V, Svensson G, Holtslag A, Meneveau C, Parlange MB (2010) Impact of surface flux formulations and geostrophic forcing on large-eddy simulations of diurnal atmospheric boundary layer flow. J Appl Meteorol Climatol 49:1496–1516

Lothon M, Lenschow DH (2011) Studying the afternoon transition of the planetary boundary layer. Eos, Trans Am Geophys Union 91:253–254

Lothon M, Lohou F, Pino D, Couvreux F, Pardyjak ER, Reuder J, Vilà-Guerau de Arellano J, Durand P, Hartogensis O, Legain D, Augustin P, Gioli B, Faloona I, Yagüe C, Alexander DC, Angevine WM, Bargain E, Barrié J, Bazile E, Bezombes Y, Blay-Carreras E, van de Boer A, Boichard JL, Bourdon A, Butet A, Campistron B, de Coster O, Cuxart J, Dabas A, Darbieu C, Deboudt K, Delbarre H, Derrien S, Flament P, Fourmentin M, Garai A, Gibert F, Graf A, Groebner J, Guichard F, Jimenez Cortes MA, Jonassen M, van den Kroonenberg A, Lenschow DH, Magliulo V, Martin S, Martinez D, Mastrorillo L, Moene AF, Molinos F, Moulin E, Pietersen HP, Piguet B, Pique E, Román-Cascón C, Rufin-Soler C, Saïd F, Sastre-Marugán M, Seity Y, Steeneveld GJ, Toscano P, Traullé O, Tzanos D, Wacker S, Wildmann N, Zaldei A (2014) The BLLAST field experiment: Boundary-Layer Late Afternoon and Sunset Turbulence. Atmos Chem Phys 14:10,931–10,960

Mahrt L (1999) Stratified atmospheric boundary layers. Boundary-Layer Meteorol 90:375–396

Mahrt L, Sun J, Blumen W, Delany T, Oncley S (1998) Nocturnal boundary-layer regimes. Boundary-Layer Meteorol 88:255–278

Monin AS, Obukhov AM (1954) Basic laws of turbulent mixing in the surface layer of the atmosphere. Contrib Geophys Inst Acad Sci 24:163–187

Nadeau DF, Pardyjak ER, Higgins CW, Fernando HJS, Parlange MB (2011) A simple model for the afternoon and early evening decay of convective turbulence over different land surfaces. Boundary-Layer Meteorol 141:301–324

Nieuwstadt FTM, Brost RA (1986) The decay of convective turbulence. J Atmos Sci 43:532–546

Pino D, Vilà-Guerau de Arellano J, Duynkerke PG (2003) The contribution of shear to the evolution of a convective boundary layer. J Atmos Sci 60:1913–1926

Pino D, Jonker HJJ, Arellano JVGD, Dosio A (2006) Role of shear and the inversion strength during sunset turbulence over land: Characteristic length scales. Boundary-Layer Meteorol 121:537–556

Rizza U, Miglietta M, Degrazia G, Acevedo O, Marques Filho E (2013) Sunset decay of the convective turbulence with Large-Eddy Simulation under realistic conditions. Physica A 392:4481–4490

Sorbjan Z (1997) Decay of convective turbulence revisited. Boundary-Layer Meteorol 82:503–517

Stull R (1988) An Introduction to Boundary Layer Meteorology. Springer Science, pp 11–23

Taylor AC, Beare RJ, Thomson DJ (2014) Simulating dispersion in the evening-transition boundary layer. Boundary-Layer Meteorol 153:389–407

Vickers D, Mahrt L (1997) Quality control and flux sampling problems for tower and aircraft data. J Atmos Ocean Technol 14:512–526

Webb EK, Pearman GI, Leuning R (1980) Correction of flux measurements for density effects due to heat and water vapour transfer. Q J R Meteorol Soc 106:85–100

Wilczak JM, Oncley SP, Stage SA (2001) Sonic anemometer tilt correction algorithms. Boundary-Layer Meteorol 99:127–150

Wyngaard JC, Coté OR, Izumi Y, Arya SPS (1972) Local free convection, similarity, and the budgets of shear stress and heat flux. J Atmos Sci 29:1230–1231